

FULL PAPER

Structural ordering of SiO₂ glass exhibiting different fictive temperatures

Hirokazu Masai^{1,†}, Yohei Onodera², Yasuhiro Fujii^{3,4}, Hideaki Hagihara⁵, Kazuya Saito⁶, Edison Sekiya⁶, Nanami Misawa⁷, Akitoshi Koreeda⁷ and Shinji Kohara²

¹National Institute of Advanced Industrial Science and Technology, 1–8–31 Midorigaoka, Ikeda, Osaka 563–8577, Japan

²Center for Basic Research on Materials, National Institute for Materials Science, 1–2–1 Sengen, Tsukuba, Ibaraki 305–0047, Japan

³Institute for Open and Transdisciplinary Research Initiatives, The University of Osaka, 2–1 Yamada-Oka, Suita, Osaka 565–0871, Japan

⁴Research Organization of Science and Technology, Ritsumeikan University, 1–1–1 Noji-higashi, Kusatsu, Shiga 525–8577, Japan

⁵National Institute of Advanced Industrial Science and Technology, 1–1–1 Higashi, Tsukuba, Ibaraki 305–8560, Japan

⁶Toyota Technological Institute, 2–12–1 Hisakata, Tempaku-ku, Nagoya 468–8511, Japan

⁷Department of Physical Sciences, Ritsumeikan University, 1–1–1 Noji-higashi, Kusatsu, Shiga 525–8577, Japan

The physical and structural parameters of glass depend on its preparation conditions. Fictive temperature, T_f , is a standard for glass obtained from the super-cooled liquid. Although the T_f value is discussed from the viewpoint of structural relaxation defined by infrared vibration, there should be structural correlations at the longer ranges, which are worthy of exploration. Here, we demonstrate the structural change of the intermediate range in SiO₂ glasses with different T_f values using X-ray and neutron diffraction, inelastic light scattering, and positron annihilation spectroscopy. By annealing the SiO₂ glasses, i.e., decreasing T_f , an increase in the first sharp diffraction peak (FSDP) heights and narrowing of the peak width are observed. Differential structure factor $\Delta S(Q)$ of neutron diffraction reveals a formation of the thermally derived O–O inter-tetrahedral correlation in high- T_f glass. Spectroscopic analyses (Raman scattering, stimulated Brillouin scattering, and positron annihilation spectroscopy) suggest that a certain structural change has occurred in the SiO₂ glass exhibiting higher T_f values, confirming that these approaches can be used as probes for structural ordering. Considering $\Delta S(Q)$ of neutron diffraction, it is suggested that the structural changes in SiO₂ glass with higher T_f values observed by spectroscopy correlate with oxygen-related structural change in the intermediate range. Since the observed structures of each analysis are different, these multiscale and quantitative examinations are important for precise examination of various random materials.

Key-words : SiO₂ glass, Fictive temperature, X-ray diffraction, Neutron diffraction, Spectroscopy

[Received October 31, 2025; Accepted December 29, 2025]

1. Introduction

As oxide glass is a solidified supercooled liquid, the thermodynamically metastable structures and physical properties of the resultant glass depend on the preparation process.^{1,2)} For example, the valence and local coordination states of the constituent cations and homogeneity of the glass melt are affected by the preparation process, even though the nominal chemical composition is fixed.³⁾ Therefore, the physical properties of oxide glass originate from how the supercooled liquid is treated above the glass transition temperature, T_g , which is a threshold for the diffusion of constituent atoms. Although it is difficult to

examine all local coordination states in glass because of the “random network” in the long-range possessing a much wider site distribution compared with that in corresponding crystal, such topological homogeneity is important for glass science from both scientific and industrial viewpoints. Recently, experimental and mathematical approaches were combined to investigate the behavior of rings and cavities in amorphous materials.^{4–10)} However, although SiO₂ glass is the most popular and typical oxide glass, the random network over the entire structural range has not yet been clarified. The random network, therefore, still fascinates many scientists.

The structural ordering of SiO₂ glass has been discussed using various structural analysis techniques. The most common method is neutron or X-ray diffraction measurement.^{1–29)} A slightly sharp peak observed in structure factor has been focused as a probe for evaluating the structural ordering in the intermediate range. For example,

[†] Corresponding author: H. Masai; E-mail: hirokazu.masai@aist.go.jp

^{*} Preface for this article: DOI <https://doi.org/10.2109/jcersj2.134.P4-1>

it is proposed that some periodic local atomic density fluctuations correlate with the first sharp diffraction peak (FSDP).¹⁰⁾ Since glass, especially SiO₂ glass, contains large cavities, the thermodynamically metastable structures can be tuned semipermanently or transiently by applying higher pressure.^{3,20–24)} In oxide glasses, in which various metastable structures exist, structural relaxation is one of the most interesting topics from both a scientific and industrial perspective.

Other probes for evaluating the structural ordering of glassy materials are spectroscopy, which is commonly non-destructive measurement of the materials, and the precise numerical analysis is an advantage for the analysis method. To examine the relationship between the cooling rate and frozen state of supercooled liquid, the concept of fictive temperature, T_f , was introduced.^{30–32)} The T_f has long been a subject of research, and its correlation has been discussed by various scientists.^{30–43)} The value of T_f , which is determined by the Si–O–Si vibration mode,³⁴⁾ is the fictive frozen state of glass and is one of the standards for structural relaxation, i.e., local structural rearrangement. The decrease of T_f means that structural relaxation of the SiO₂ glass occurs by annealing. Changes in fictive temperature not only change the wave number of Si–O–Si vibrations but also affect a wide range of physical properties, such as the elastic modulus, thermal expansion coefficient, and chemical durability. On the one hand, this effect is complex; some parameters increase, while others decrease. This is attributable to the fact that different structures at different distance ranges contribute to different physical properties.

On the other hand, inelastic light scattering has been used as a spectroscopic probe for structural ordering.^{1–3,25,26,44–49)} In particular, the range of wavenumbers below 50 cm^{−1} in inelastic light scattering is conventionally called the boson region, at which a peak above the density of state estimated by the *Debye rule* in glass (random material) emerges. A correlation between the boson peak and FSDP has been discussed by many authors from viewpoint of structural ordering.²⁷⁾ In addition, we have recently demonstrated other spectroscopic methods such as Brillouin scattering and positron annihilation spectroscopy can be a probe to examine the structural ordering of glasses.⁴⁹⁾ Since many rings of different sizes exist in SiO₂ glasses,^{5,7,8)} it is natural that cavities inevitably generated from rings affect the nature of SiO₂ glass. Therefore, a quantitative understanding of cavities, which are characteristic of glass, is important. The structural ordering of the glass network has been often discussed by limited analytic methods, i.e., a certain distance ranges. However, since structural ordering in a specific structural range should affect the ordering of other ranges, it is preferable to use many analytical techniques to evaluate non-periodic glass networks.

In this study, we examined the structural ordering of SiO₂ glasses exhibiting different T_f values by different analysis methods: FSDP of high-energy X-ray diffraction and neutron diffraction, boson peak in Raman scattering, Brillouin scattering, and positron annihilation spectroscopy.

By using these analyses, we examined the structural changes in the entire SiO₂ network by thermal relaxation using numerical values.

2. Experimental

2.1 Preparation of SiO₂ glasses possessing different T_f values

The base SiO₂ glass was supplied by Tosoh Quartz Corp. The OH concentration was <50 wt. ppm. The preparation details have been presented in a previous paper.²⁹⁾ To examine the stimulated Brillouin scattering, the edges of the samples were polished to obtain a mirror surface.

2.2 Physicochemical analysis

Density was estimated according to a previous report.⁵⁰⁾ The refractive index of the samples was measured using a prism coupler (Metricon, N.J., U.S.A.) at 473, 633, and 1319 nm. The error of the measurement was 3×10^{-4} . T_f was estimated by the Si–O–Si vibration around 2260 cm^{−1} using a Model Spectrum 2000 (Perkin Elmer Inc.) with a resolution of 1 cm^{−1}.

2.3 High-energy XRD measurement

The high-energy X-ray diffraction experiment was performed at the BL04B2 beamline at the SPring-8 synchrotron radiation facility using a two-axis diffractometer dedicated to the study of disordered materials.⁵¹⁾ The energy of the incident X-rays was 61.43 keV. The raw data were corrected for polarisation, absorption, and background, and the contribution of Compton scattering was subtracted using standard data analysis software.⁵¹⁾ The corrected X-ray diffraction data were normalized to give the Faber–Ziman⁵²⁾ X-ray total structure factors, $S^X(Q)$.

2.4 Neutron diffraction measurement

Neutron diffraction measurements were conducted using a high-intensity total diffractometer (NOVA) installed at BL21 of the Materials and Life Science Experimental Facility at the J-PARC spallation neutron source (Ibaraki, Japan). The wavelength range of the incident neutron beam was $0.12 \text{ \AA} < \lambda < 8.3 \text{ \AA}$. The glass sample (1.2 g) was transferred into a vanadium–nickel null alloy cell with an outer diameter of 6.0 mm and thickness of 0.1 mm. The observed scattering intensity for the sample was corrected for instrumental background and attenuation of the sample and cell, and then, normalized by the incident beam profile obtained from the scattering intensity of a vanadium standard. The corrected neutron diffraction data were normalized to give the Faber–Ziman⁵²⁾ neutron total structure factors, $S^N(Q)$.

2.5 Raman spectroscopy

Confocal micro-Raman measurements with a backscattering geometry were performed to analyse the boson peaks. Backscattering micro-Raman measurements were performed using a single-frequency diode-pumped solid-state (DPSS) laser oscillating at 532 nm (Oxxius LCX-532S-300). A home-built microscope consisting of ultra-narrow

band notch filters (OptiGrate) and a 20× objective lens (Mitutoyo, M Plan APO SL20, NA = 0.28) was used to focus the excitation laser and collect the Raman-scattered light. The scattered light was analysed using a single monochromator (Jovin-Yvon, HR320, 1200 grooves/mm) equipped with a charge-coupled device camera (Andor, DU420).

2.6 Stimulated Brillouin spectroscopy

Brillouin shifts ν_B of the glass were measured using a frequency-modulated stimulated Brillouin spectrometer.^{53,54} Two Miser-type Nd:YAG lasers with a wavelength of 1.06 μm were utilized as pump and probe sources. The beams were arranged in a counterpropagating configuration within the sample, enabling a backscattering geometry. The frequency difference between the pump and probe waves, along with the resulting beat frequency, was continuously monitored using a microwave frequency counter. This setup facilitated repetitive scanning and data averaging while preserving high spectral resolution. By employing two lenses with a focal length of 30 cm, a spectral resolution of 20 kHz (HWHM) was achieved. The longitudinal sound velocity V_L was calculated using the relation $V_L = \nu_B \lambda / 2n_{1064}$, where ν_B , λ , n_{1064} , are the Brillouin shift, the wavelength of the incident light (= 1064 nm), and the refractive index at 1064 nm, respectively. The n_{1064} values were calculated using the Cauchy relation with the refractive indices at different wavelengths.

2.7 Positron annihilation lifetime measurement

Positron annihilation lifetime measurements were performed using a PSA TypeL-II (Toyo Seiko Co. Ltd.) with an anti-coincidence system.⁵⁵ The ²²Na source with a diameter of 15 mm was encapsulated with Kapton® film. The accumulated count for each sample was 10⁷.

3. Results

3.1 Comparison of the X-ray and neutron structure factors $S(Q)$ of SiO₂ glasses exhibiting different T_f values

Figures 1(a) and 1(b) show the X-ray total structure factors $S^X(Q)$ ²⁹ and neutron total structure factors $S^N(Q)$ of SiO₂ glasses with different T_f values, respectively. The FSDP (Q_1)^{3,5,7,22–24} is clearly observed at approximately $Q = 1.5 \text{ \AA}^{-1}$ in both $S^X(Q)$ and $S^N(Q)$. On the contrary, a principal peak (PP) (Q_2)^{3,5,7,22–24} at approximately $Q = 2.9 \text{ \AA}^{-1}$ is only observable in neutron diffraction data because the O–O correlation, which is probed sensitively by neutrons, mainly contributes to this peak.^{5,7,22,23} The peak attributed to Q_3 is observed at $Q = 5.1 \text{ \AA}^{-1}$ [$S^X(Q)$]^{3,24} and at $Q = 5.3 \text{ \AA}^{-1}$ [$S^N(Q)$]^{3,5,7,22–24} respectively. These three peaks slightly altered their shape depending on the T_f value. Figures 1(c) and 1(d) show the enlarged $S^X(Q)$ and $S^N(Q)$ of SiO₂ glasses with different T_f values in the FSDP region. Each inset shows the FSDP height of the SiO₂ glasses as a function of T_f . The height of the FSDP linearly

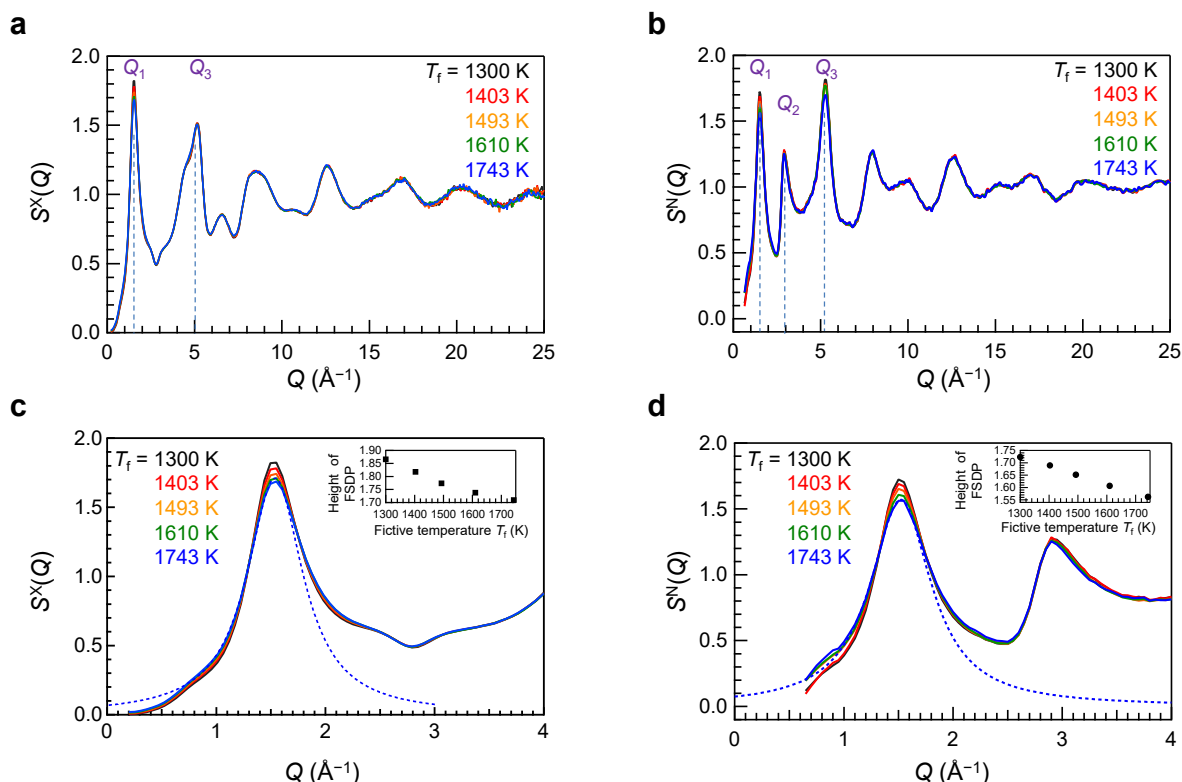


Fig. 1. Comparison of the X-ray and neutron total structure factors $S(Q)$ of SiO₂ glasses exhibiting different T_f values. (a) X-ray total structure factors $S^X(Q)$ ²⁹ and (b) neutron total structure factors $S^N(Q)$ of SiO₂ glasses exhibiting different T_f values. Enlarged $S^X(Q)$ ²⁹ (c) and $S^N(Q)$ (d) at the FSDP region with the fitting curve (dotted line). Insets of Figs. 1(c) and 1(d) show the heights of FSDP as a function of T_f values.

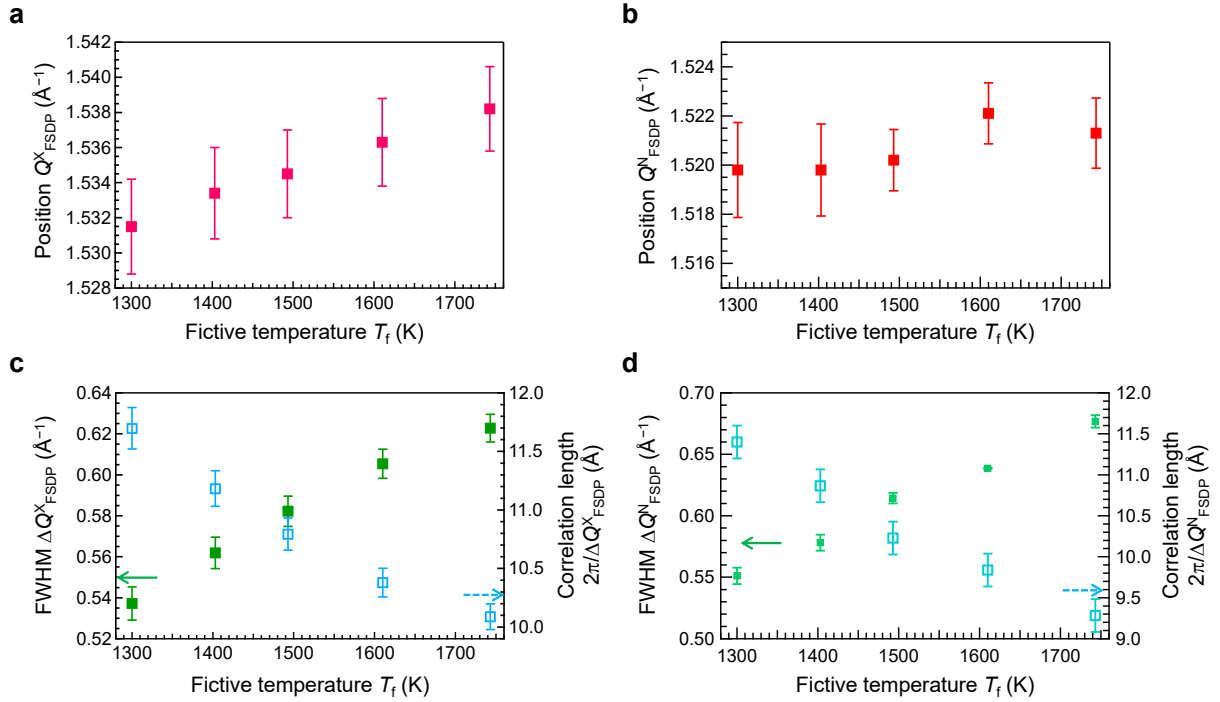


Fig. 2. The fictive temperature (T_f) dependence of the FSDP in the X-ray and neutron diffraction data of SiO_2 glasses. Position of the FSDP in $S^{\text{X}}(Q)^{29}$ (a) and $S^{\text{N}}(Q)$ (b). (c) Full width half maximum (FWHM) of the FSDP in $S^{\text{X}}(Q)$, $\Delta Q_{\text{FSDP}}^{\text{X}}$, and the correlation length $2\pi/\Delta Q_{\text{FSDP}}^{\text{X}}$ as a function of T_f .²⁹⁾ (d) FWHM of the FSDP in $S^{\text{N}}(Q)$, $\Delta Q_{\text{FSDP}}^{\text{N}}$, and the correlation length $2\pi/\Delta Q_{\text{FSDP}}^{\text{N}}$ as a function of T_f .

increased with decreasing T_f values, indicating that structures correlated with the FSDP were preferentially ordered by thermal annealing.^{18,19,28,29)} To examine the effect of T_f on the structural ordering in SiO_2 glass more quantitatively, the FSDP was fitted using a Lorentz function taking into account the position, Q_{FSDP} , and full width at half maximum (FWHM), ΔQ_{FSDP} , of the FSDP:

$$S(Q) = A_0 \times \frac{0.5\Delta Q_{\text{FSDP}}}{(Q - Q_{\text{FSDP}})^2 + (0.5\Delta Q_{\text{FSDP}})^2} \quad (1)$$

where, A_0 , ΔQ_{FSDP} , and Q_{FSDP} are the fitting parameters.²⁹⁾ In this study, we fitted the $S(Q)$ in the Q regions of 0.90–1.65 \AA^{-1} for $S^{\text{X}}(Q)$ and 1.10–1.65 \AA^{-1} for $S^{\text{N}}(Q)$. The dotted curves in Figs. 1(c) and 1(d) represent the fitted curves to the FSDP of SiO_2 glass with $T_f = 1743$ K.

Figure 2 shows the fitting results of Q_{FSDP} ($Q_{\text{FSDP}}^{\text{X}}$ for X-ray and $Q_{\text{FSDP}}^{\text{N}}$ for neutron) and ΔQ_{FSDP} ($\Delta Q_{\text{FSDP}}^{\text{X}}$ for X-ray and $\Delta Q_{\text{FSDP}}^{\text{N}}$ for neutron) as a function of T_f . Compared the values of $Q_{\text{FSDP}}^{\text{X}}$ [Fig. 2(a)] with those of $Q_{\text{FSDP}}^{\text{N}}$ [Fig. 2(b)], the $Q_{\text{FSDP}}^{\text{X}}$ increases slightly with increasing T_f values²⁹⁾ whereas the $Q_{\text{FSDP}}^{\text{N}}$ remains almost identical. On the other hand, the FSDP width becomes broader in both $S^{\text{X}}(Q)$ and $S^{\text{N}}(Q)$ [Figs. 2(c) and 2(d)]. The diversity of the FSDP-related structure was evaluated by examining the correlation length, $2\pi/\Delta Q_{\text{FSDP}}$, as a function of T_f [Figs. 2(c) and 2(d)]. The correlation length obtained from both $S^{\text{X}}(Q)$ and $S^{\text{N}}(Q)$ increases by thermal annealing (a decrease in T_f), suggesting that annealing induces the structural ordering consists of SiO_4 network.

The X-ray and neutron $S(Q)$ of SiO_2 glass exhibited

slightly different behavior in response to the T_f values, as shown in Figs. 1 and 2. In order to characterize the different behavior, we calculated the differential $S(Q)$, $\Delta S(Q)$, for both $S^{\text{X}}(Q)$ and $S^{\text{N}}(Q)$; Using the $S(Q)$ of SiO_2 glass with the $T_f = 1300$ K as the reference data, $\Delta S(Q)$ was obtained by subtracting the reference data from the $S(Q)$ of SiO_2 glasses with the other T_f values (1403, 1493, 1610, and 1743 K). **Figures 3(a) and 3(b)** show the X-ray and neutron $\Delta S(Q)$ of SiO_2 glasses. In both X-ray and neutron $\Delta S(Q)$, the clear changes corresponding to the T_f values were observed at the Q_1 , Q_2 , and Q_3 regions. To clarify the origin of the changes in each diffraction peak, the X-ray- and neutron-weighted partial structure factors $W_{ij}(Q) \cdot S_{ij}(Q)$ of Si–Si, Si–O, and O–O are shown in bottom of Figs. 3(a) and 3(b), respectively. In disordered materials containing n chemical species, the total structure factor $S(Q)$ can be expressed using the X-ray or neutron weighting factors, $W_{ij}(Q)$, and partial structure factors, $S_{ij}(Q)$, for i - j correlations,

$$\begin{aligned} S(Q) &= \sum_{i=1}^n \sum_{j=1}^n W_{ij}(Q) \cdot [S_{ij}(Q) - 1] \\ &= 1 + \frac{1}{\langle f(Q) \rangle^2} \sum_{i=1}^n \sum_{j=1}^n c_i c_j f_i(Q) f_j(Q) [S_{ij}(Q) - 1] \end{aligned} \quad (2)$$

where c_i is the atomic fraction of chemical species i , and $f_i(Q)$ is either a Q -dependent atomic form factor in X-ray diffraction or a Q -independent coherent scattering length in neutron diffraction, and

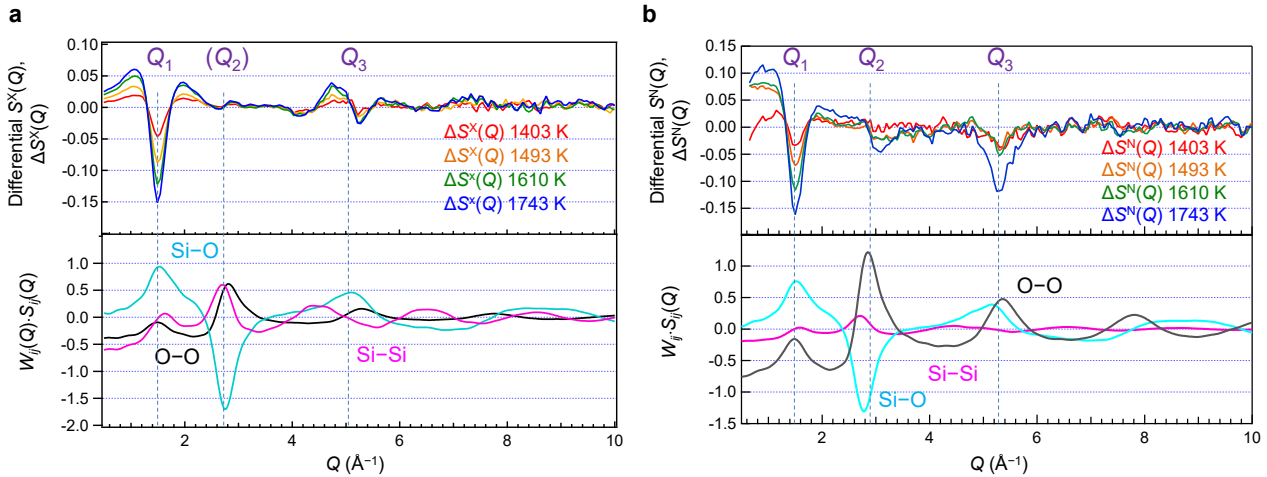


Fig. 3. Comparison of the X-ray and neutron differential structure factors $\Delta S^{X,N}(Q)$ of SiO₂ glasses exhibiting different T_f values. (a) $\Delta S^X(Q)$ and (b) $\Delta S^N(Q)$, which are obtained by subtracting $S(Q)$ of SiO₂ glass with the $T_f = 1300$ K (reference data) from $S(Q)$ of SiO₂ glasses with the other T_f values (1403, 1493, 1610, and 1743 K). X-ray-weighted partial structure factors $W_{ij}(Q) \cdot S_{ij}(Q)$ and neutron-weighted partial structure factors $W_{ij} \cdot S_{ij}(Q)$ are also presented at the bottom of each figure. Vertical dot lines indicate Q values of each Q_n peak.

$$\langle f(Q) \rangle = \sum_{i=1}^n c_i f_i(Q) \quad (3)$$

The $S_{ij}(Q)$ data were calculated from the three-dimensional atomic configuration of SiO₂ glass, which was constructed by a combination of molecular dynamics (MD) and reverse Monte Carlo (RMC) simulations based on X-ray and neutron diffraction data.⁵⁾ Further details of the MD-RMC simulations of SiO₂ glass are described in Ref. 5).

As previously reported,²⁹⁾ the $\Delta S^X(Q)$ is mainly dominated by the Si-Si and Si-O correlations. For instance, the Si-Si and Si-O correlations contribute to Q_1 and Q_3 regions in the $\Delta S^X(Q)$ [bottom of Fig. 3(a)] because X-rays are more sensitive to heavier atoms. The $\Delta S^X(Q)$ exhibits a negative peak at the $Q_{\text{FSDP}} (= 1.5 \text{ \AA}^{-1})$, and the depth of this negative peak increases uniformly with increasing T_f , associated with the increases on both the lower- and higher- Q sides of the FSDP. This change signifies the FSDP's systematic broadening indicating that the intermediate-range structure becomes disordered with increasing T_f . This behavior is consistent with the correlation length analysis results showing that annealing (lowering T_f) induces structural ordering in SiO₂ glass. The Q_3 exhibited contrary alterations in direction between the lower- and higher- Q sides in the $\Delta S^X(Q)$. This behavior in the Q_3 is consistent with that in the Si-Si partial structure factor [see $W_{ij}(Q) \cdot S_{ij}(Q)$]; the Si-Si correlation corresponds to the correlation between central Si atoms located in SiO₄ tetrahedra interconnected by corner-sharing of oxygen atoms in SiO₂ glass. The change in the Q_3 in the $\Delta S^X(Q)$ suggests that the annealing process affects the Si-O-Si correlation in SiO₂ glass.²⁹⁾ In contrast to the Q_1 and Q_3 , the Q_2 exhibited no signs of change in the $\Delta S^X(Q)$ since the positive Si-Si and O-O contributions are counterbalanced by the negative Si-O contribution in the Q_2 region.

The $\Delta S^N(Q)$ [Fig. 3(b)] exhibited changes in three diffraction peaks, including the Q_2 , in contrast to the $\Delta S^X(Q)$. The Q_1 (FSDP) in the $\Delta S^N(Q)$ demonstrates a change identical to that in the $\Delta S^X(Q)$, though the lower- Q side underwent a more significant alteration. This can be attributed to the fact that O-O correlation, which contributes to the lower- Q side of the Q_1 has a large weighting factor in neutron diffraction as shown in $W_{ij} \cdot S_{ij}(Q)$ in comparison with the Si-Si correlation. The positive contributions are observed for the neutron-weighted O-O partial structure factor in the Q_2 and Q_3 regions. Notably, the higher- Q side of the Q_2 in the $S^N(Q)$ is predominantly formed by the O-O correlation contribution. Thus, the evolution of the negative peak observed at $Q = 3.1 \text{ \AA}^{-1}$ in the $\Delta S^N(Q)$ can be attributed to the diminution of the Q_2 in the O-O partial structure factor, suggesting that oxygen-related structural disordering occurs as the T_f values increase. The Q_2 peak in oxide glasses is correlated with the packing of oxygen atoms at the corner of polyhedral units (e.g., SiO₄ tetrahedron in SiO₂ glass).³⁾ Since the network structure of interconnected regular SiO₄ tetrahedra is preserved in SiO₂ glasses with different T_f values, we suggest that inter-tetrahedral O-O correlation^{3,22,23)} plays a major role in the oxygen-related structural disordering that occurs as the T_f increases.

3.2 Spectroscopic analysis of SiO₂ glass exhibiting different T_f values

Recently, we have examined network structure of glass through a combination of diffraction and spectroscopic techniques. It is found that inelastic light scattering (Raman and Brillouin scattering) and positron annihilation spectroscopy can be a probe of structural diversity of oxide glass in addition to the high energy XRD and solid state magic angle spinning NMR.⁴⁹⁾ **Figure 4(a)** shows the Raman spectra in the boson region of SiO₂ glass exhibiting

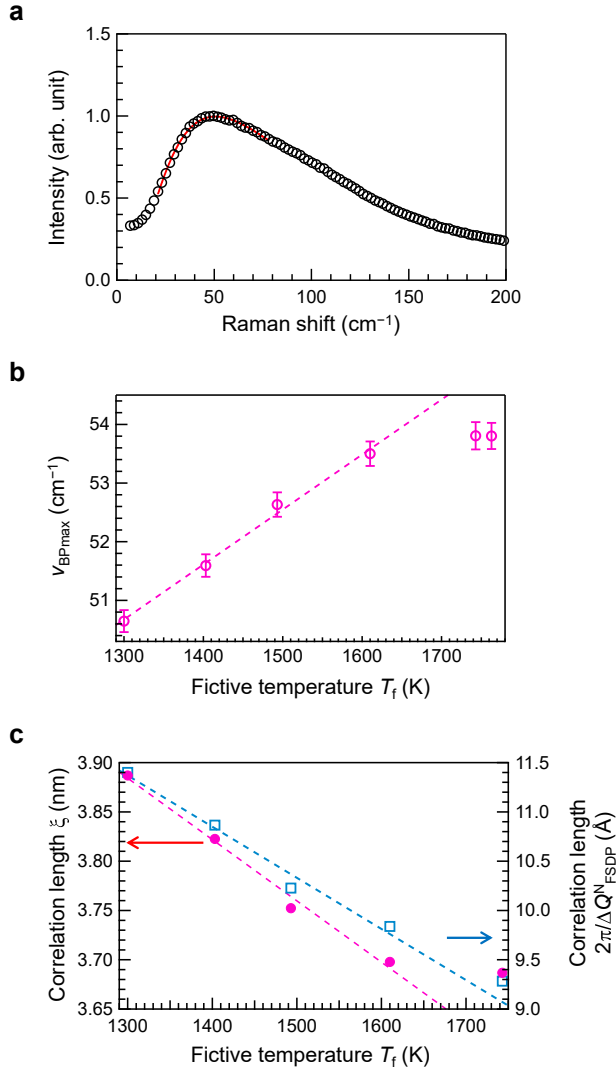


Fig. 4. Raman spectra of SiO₂ glass exhibiting different T_f values. (a) Raman scattering spectra at boson region of SiO₂ glass exhibiting $T_f = 1300$ K as a representative. (b) ν_{BPmax} as a function of T_f values. (c) Comparison of size parameters from boson peak and correlation length $2\pi/\Delta Q^N_{FSDP}$ as a function of T_f values.

the $T_f = 1300$ K, as a representative. All Raman spectra of SiO₂ glasses exhibiting different T_f values are shown in Fig. S1. We adopted a standard procedure to analyse Boson peaks with a log-normal function, i.e., the shape of the reduced spectrum is assumed to be the form given in Eq. (4).^{46–48)}

$$\frac{\chi''(\nu)}{\nu} = \frac{A}{\sqrt{2\pi}\sigma\nu} \exp\left(-\frac{(\ln \nu - \mu)^2}{2\sigma^2}\right), \quad (4)$$

where, ν , A , e^μ , and σ are the frequency shift, amplitude, median of the log-normal distribution, and standard deviation of the Gaussian peak in log-space, respectively. The values of the ν_{BPmax} were calculated as $e^{\nu-\sigma^2}$ using fitting results. The values of ν_{BPmax} are plotted as a function of T_f in Fig. 4(b). The ν_{BPmax} shifts to the low-frequency side as T_f decreases, and the amount of ν_{BPmax} change is approximately 5%. Although the data initially suggest a linear

trend, a minor deviation from linearity becomes evident for SiO₂ glass with higher T_f value. If all data are used for linear fitting, the coefficient of determination (R^2) for the linear regression becomes 0.944, while the R^2 value becomes 0.993 with the fitting using lower 4 data.

It has been reported that there is a relationship among frequency of boson peak ν_{BPmax} , sound velocity v , and correlation length ξ , as shown in Eq. (5).^{46–48)}

$$\xi \sim v/\nu_{BPmax} \quad (5)$$

As shown in Fig. 4(b), the boson peak frequency decreases with decreasing T_f . After annealing, which induces a decrease in T_f , the spectral change indicated that the correlation length increased. Figure 4(c) shows the T_f dependence of the correlation length ξ calculated using Eq. (5). The correlation length calculated from the value of FSDP of neutron diffraction is also shown for comparison. In contrast to the linear relationship observed in the FSDP value, a minor deviation from linearity of the boson peak position is observed owing to the ν_{BPmax} . The change rates in the T_f range of 1300 to 1610 K of boson peak and FSDP are -1.57×10^{-2} and $-4.42 \times 10^{-2} \%$ /K, respectively. As reported in previous papers, there is a relationship between the positions of the boson peak and FSDP,⁴⁸⁾ whereas the boson peak position and density, i.e., FSDP position, exhibit a non-linear dependence in a densified SiO₂ glass.³⁾ As in the previous paper,³⁾ the present results, in which a deviation is observed in higher T_f glass, suggest that the relationship between positions of boson peak and FSDP does not follow a linear correspondence.

As in previous studies,⁵⁶⁾ Brillouin spectra have been used to determine the sound velocity and elastic modulus of materials. In our previous study,²⁹⁾ Brillouin spectra were fitted using the Voigt function to calculate the Brillouin shifts ν_B of SiO₂ glass samples against different T_f values. Although an apparent linearity was observed between the c_{11} and T_f values in the previous paper,²⁹⁾ the conventional Brillouin measurement cannot be used for quantitative analysis of the Brillouin peak width of SiO₂ glass exhibiting different T_f values, because Brillouin peak width of SiO₂ is narrower compared with other oxide glasses.⁴⁹⁾ We, therefore, examined the structural ordering employing stimulated Brillouin scattering approach with a phase modulation. The details of the analysis are shown in the previous paper.⁵⁴⁾

The stimulated Brillouin scattering spectra were fitted by the real and imaginary parts of the frequency-modulated Lorentzian functions as presented in Eq. (1) of Ref. 51) only with the electrostrictive coupling. Since the wavelength of the laser employed is twice that we reported previously, the Brillouin shift in this study is approximately halved. Figure S2 shows the refractive index at 1064 nm, which corresponds to the wavelength used for stimulated Brillouin scattering. With decreasing T_f , the refractive index decreases. **Figures 5(a) and 5(b)** show the stimulated Brillouin scattering spectra of SiO₂ glasses exhibiting different T_f values of the real part (a) and imaginary part (b). The spectra of the real and imaginary parts

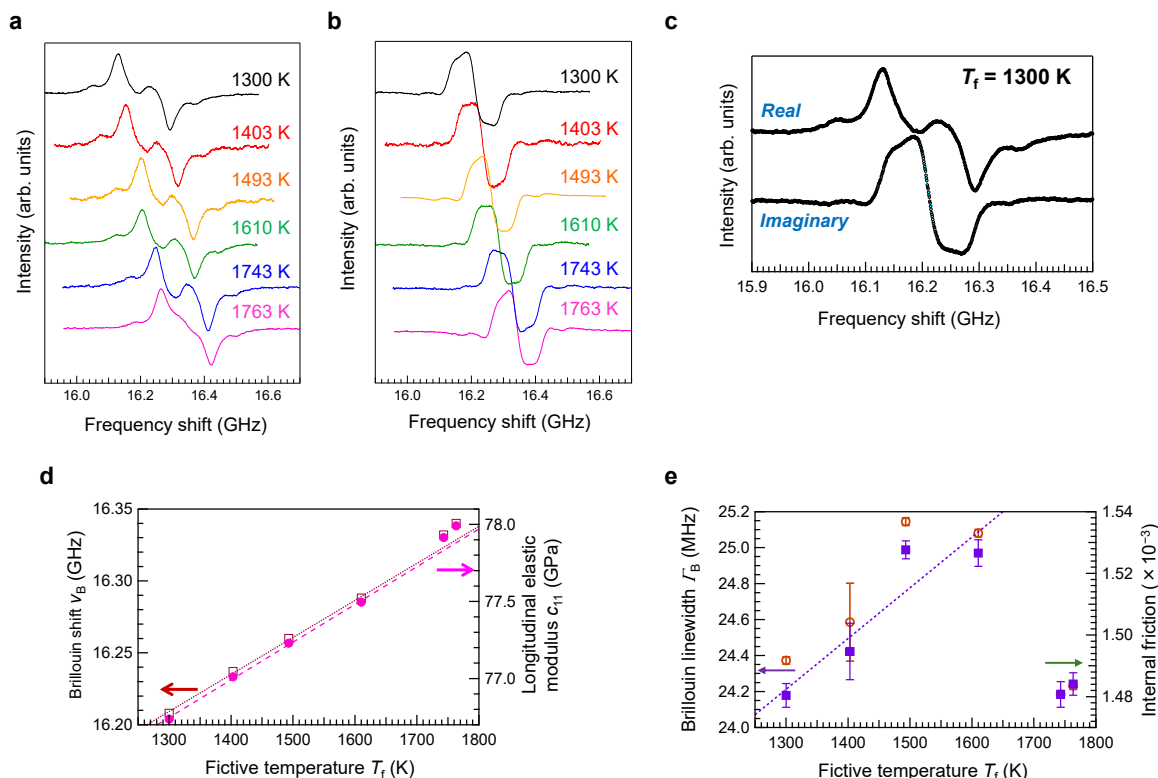


Fig. 5. Stimulated Brillouin scattering spectra of SiO₂ glass depending on T_f values. Stimulated Brillouin scattering spectra of SiO₂ glasses exhibiting different T_f values; the real part (a) and imaginary part (b). (c) Fitting of stimulated Brillouin scattering spectra. Circles and solid lines are experimental and fitted data, respectively. (d) T_f dependence of Brillouin shift ν_B and longitudinal elastic modulus c_{11} as a function of T_f . (e) Brillouin peak width Γ_B and internal friction of SiO₂ glass possessing different T_f values.

can be fitted by the frequency-modulated Lorentzian response functions as shown in Fig. 5(c). The theoretical curves exhibit excellent agreement with the experimental data, enabling us to accurately determine the Brillouin shift and linewidth. The longitudinal elastic modulus c_{11} values were calculated, as shown in Eq. (6),

$$c_{11} = \rho(\nu_B \lambda / 2n_{1064}) \quad (6)$$

where λ , and n_{1064} are the Brillouin shift, the wavelength of the incident light (1064 nm), and the refractive index at 1064 nm, respectively. Figure 5(d) shows the Brillouin shift ν_B and the longitudinal elastic modulus c_{11} as a function of T_f values. There appears to be a linear relationship between T_f and these two parameters. On the contrary, the T_f dependence of the Brillouin peak width Γ_B exhibits a quite different tendency, as shown in Fig. 5(e): the Γ_B reaches its maximum when the T_f is approximately 1600 K, and then decreases. Generally, peak width Γ_B becomes narrower with increasing frequency. The internal friction, which is defined as Γ_B/ν_B , of this SiO₂ glass, is also shown in Fig. 5(e) as a function of T_f . Because the change in Γ_B ($\sim 5\%$) is larger than that in ν_B ($\sim 1\%$), this confirms that the size change of correlation length is meaningful. Thus, the obtained data suggest that not only the Brillouin peak width, but also internal friction do not show a linear dependence on temperature, and these parameters

decrease in SiO₂ glasses exhibiting higher T_f values ($T_f > 1700$ K). Since Brillouin peak width is proportional to the ultrasonic attenuation the decrease of Γ_B indicates a qualitative change in the phonon scattering mechanism in the length scale of micrometer order across $T_f \sim 1700$ K. Regarding the refractive index, we believe it does not affect either the Raman or the Brillouin results. The boson peak, which reflects the vibrational density of states, is generally considered to be independent of the refractive index. Since no irregularity originating from the refractive index has been observed, we can conclude that the slight change in the refractive index ($< 0.05\%$) is negligible in the estimation of the c_{11} value, because the Brillouin shift itself shows a variation of about 1 %.

Since it is expected that internal friction of SiO₂ glasses correlates with the cavity of SiO₄ network, we performed positron annihilation lifetime spectroscopy to quantify the cavity size in materials.^{57–59)} Figure 6(a) shows the positron decay curves of the SiO₂ glass with different T_f values, where there is a slight difference in these curves. For insulators, the decay constant of ortho-positronium *o*-Ps (the third component in fitting the decay curve) was used for the size calculation. Figure 6(b) shows lifetime of *o*-Ps (on the left axis) and the relative intensity of total decay components (on the right axis) as a function of T_f values. Both lifetime and intensity exhibit an inflection point at

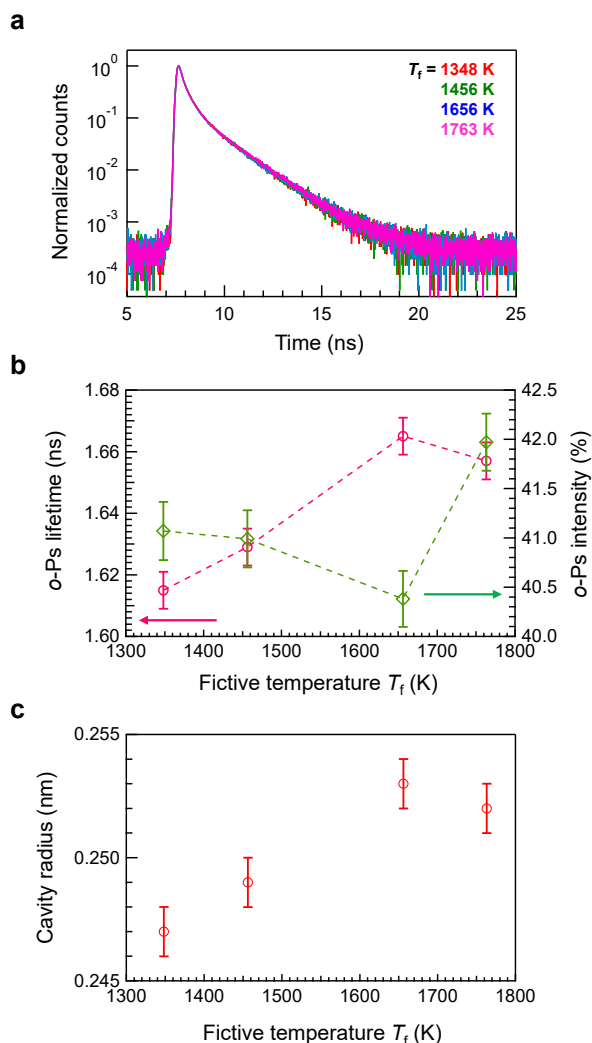


Fig. 6. Positron annihilation lifetime spectroscopy for determination of cavity of SiO₂ glasses exhibiting different T_f values. (a) Positron decay curves of SiO₂ glasses exhibiting different T_f values. (b) Lifetime of ortho-positronium (o-Ps) τ_3 and the intensity I_3 as a function of a function of T_f values. (c) Correlation between cavity radius and T_f of SiO₂ glasses.

the SiO₂ glass whose T_f is 1656 K. The cavity radii of this SiO₂ glass are plotted in Fig. 6(c) as a function of the T_f values. Although preliminary observations suggest an apparent consistency between cavity sizes of SiO₂ and T_f values in the previous literatures; the cavity size increases with increasing T_f value,⁵⁸⁾ there is a different tendency at higher T_f -glass. The anomalous change of SiO₂ glasses with higher T_f will be discussed with other spectroscopic data in the following section.

4. Discussion

In the previous paper,²⁹⁾ we assumed the T_f dependence on the structural parameters of SiO₂ glass to be linear.

As shown in T_f -dependence of the FSDP of $S^X(Q)$, the change of $S^X(Q)$, which is largely affected by the Si-related correlation, is roughly proportional to that of T_f . On the contrary, in the structure factor $S^N(Q)$, which is largely affected by the O–O correlation, the T_f -dependences of Q_n

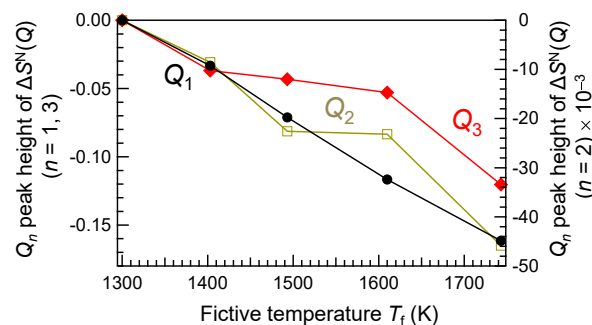


Fig. 7. Q_n peak height of $\Delta S^N(Q)$ of SiO₂ glasses as a function of T_f values.

peaks are not identical to that in $S^X(Q)$. **Figure 7** shows the Q_n peak height of $\Delta S^N(Q)$ of SiO₂ glasses exhibiting different T_f values. In the case of Q_1 (FSDP), the change is linear as observed in spectra change of $\Delta S^X(Q)$. However, for Q_2 and Q_3 peaks, a steep change is observed for SiO₂ glass with $T_f = 1743$ K. Comparing $\Delta S^N(Q)$ with $\Delta S^X(Q)$, the steep change is only observed in $S^N(Q)$. Therefore, we assume that the spectra change correlates with an oxygen-related structure. It is worth noting that the inter-tetrahedral O–O correlation observed in the present case seems to be different from that observed in densified SiO₂ glass, in which a significant density change is observed.³⁾ In contrast to pressure-driven structural change of densified glass,³⁾ thermodynamic change from the supercooled state should change by undergoing a different pathway. It is expected from the results of positron annihilation spectroscopy that the formation of a smaller ring is the result of high instability of the larger rings in higher T_f -glass.

As shown in Fig. 6(c), an inflection point of structural parameter with respect to the T_f values is also observed in positron annihilation spectroscopy. It has been reported that small-membered rings, such as three-membered rings, exist in SiO₂ glass exhibiting higher T_f values, and these rings induce higher refractive index, density, and elastic modulus.⁶⁰⁾ Meanwhile, larger cavities are formed in SiO₂ glasses exhibiting higher T_f values as a counterpart. Although cavity sizes of the present result are in accordance with those in the literature for cavities of SiO₂ with lower T_f values (<1650 K),⁵⁸⁾ the deviation from linearity is observed at the higher- T_f region. It is notable that this study is the first result to evaluate the cavity size of SiO₂ glasses with higher T_f (> 1700 K) using the positron annihilation spectroscopy. It is reported that a positron line-shape parameter of SiO₂ glass saturates after heat treatment at 1673 K.⁵⁷⁾ Although Brauer et al.⁵⁷⁾ used the positron lineshape parameter to evaluate the crystallinity of SiO₂ glass, it is suggested that the saturation behavior depending on temperature is similar to our case.

In both inelastic light scattering, while the boson peak frequency ν_{BPmax} and Brillouin shift ν_B appear to be linear at lower T_f region, a slight nonlinearity is also discernible in the high- T_f region. Here, we have compared Brillouin peak width Γ_B (Brillouin) and standard deviation of log-normal function σ (Raman) concerning to spectral broad-

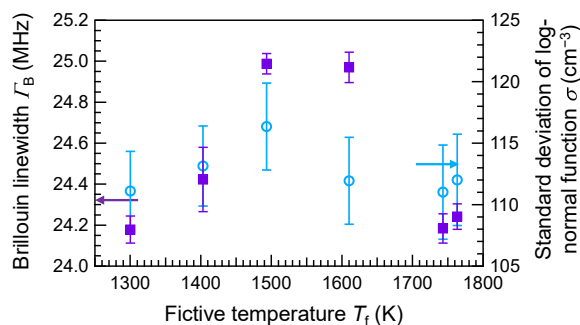


Fig. 8. Brillouin peak width Γ_B and standard deviation of log-normal function σ as a function of T_f values.

ening, i.e. the structural diversity. **Figure 8** shows Brillouin peak width Γ_B and standard deviation of log-normal function σ as a function of T_f values. In both parameters, inflection points can be observed, which suggests that some structural change occurred in SiO₂ glass with higher T_f value. In SiO₂ glass exhibiting a lower T_f value, the number of 6-membered rings (the most thermally stable structure) is increased. If there are many large-membered rings with a cavity, the refractive index and elastic modulus, which reflect the number of bridging bonds per unit volume, decrease. Such a cavity, i.e., free volume, acts as a disturbance to the phonon propagation of sound velocity, and consequently, a decrease in the propagation distance of the ultrasonic wave. The propagation distance of the ultrasonic wave is inversely proportional to Γ_B . In the present study (at approximately 33 GHz, 180 nm), the mean free path was calculated as 73 μm ($T_f = 1300$ K) and 77 μm ($T_f = 1763$ K). The values show that phonon scattering is high in SiO₂ glass with a low T_f value, indicating the formation of 6-membered rings with a significant fraction of cavities. We assume that the observed structural changes do not originate from structural heterogeneity because of the nature of experimental techniques. Although SiO₂ glasses with the T_f of more than 1700 K were rapidly quenched, the samples were polished for both spectroscopic and optical measurements. In addition, for Raman spectra, the areas close to the surface were observed whereas stimulated Brillouin spectra reflect information of bulk area. Since Raman and Brillouin spectra exhibit similar dependence on T_f , the glass can be treated as a structurally uniform medium for the purposes of this analysis. Thus, we can conclude that the thermal history affects the formation of various rings during the vitrification.

Here we discuss a plausible reason for the observed change based on a formation of 6-membered rings and other smaller- or larger-membered rings. As a 6-membered ring is the most thermally stable structure, an increase in the number of 6-membered rings will induce a decrease in site distribution as observed in SiO₂ glass with lower T_f . It is reported that both smaller- and larger-membered rings are formed with increasing T_f . The formation of various rings is reflected in the change of the Brillouin shift, the standard deviation of the boson peak, and the width of the Brillouin peak. In the case of $S^N(Q)$, a formation of structures is ob-

served at the Q region below 1 \AA^{-1} [see Figs. 1(d) and 3(b)]. In addition, T_f -dependences of peak height of $\Delta S^N(Q)$ of SiO₂ glasses are different. It is thought that the degree of ordering or disordering is determined by the difference in the distance range observed. Since the temperature dependence of Brillouin peak width is slightly different from the other spectroscopic data, it is expected that the width reflects longer-distance structure, although the distance also belongs to the intermediate-range (not the long-range ordering, i.e. crystalline structure).

Since glass possesses metastable network quenched at a certain temperature, although the actual construction of SiO₂ glass is difficult to determine because of coexistence of various non-symmetric rings, recent ring analysis allows for the visualization of plausible random network structures.^{3–10,61)} On the other hand, as shown in the present data, rearrangement of network structure upon annealing (relaxation) is still complicated. Since there is no analytical method to determine the network structure of glasses with different distance range, a combination of multiple measurement techniques is important for understanding the nature of the glass network.

5. Conclusions

Transparent SiO₂ glasses with different T_f values were examined using several measurement approaches. The HEXRD and neutron diffraction results suggest the formation of a more disordered structure in SiO₂ glass with higher T_f values, and oxygen-related species correlate the structural change. The correlation length of the boson peak showed a slightly different tendency to that of the FSDP, indicating that the structural origin of the boson peak is not the same as that of FSDP. Data from the stimulated Brillouin scattering spectra suggest that structural changes occurred in SiO₂ glass with higher T_f values, which is also detected by positron annihilation spectroscopy. We have demonstrated Brillouin peak width and standard deviation of log-normal function can be used as a probe for the structural ordering of glass. Although the direct atomistic observation of glass is very difficult, these multiscale and quantitative examinations are milestones in the evaluation of various random materials.

Acknowledgments High-energy XRD measurements were performed on the BL04B2 beamline at SPring-8 with the approval of the Japan Synchrotron Radiation Research Institute (JASRI) (Proposal Numbers 2015A1313 and 2024B1004). Neutron diffraction measurements were performed on the BL21 beamline at J-PARC with the permission from J-PARC (Proposal Number 2017A0232). This work was partially supported by the Japan Society for the Promotion of Science Grant-in-Aid for Scientific Research (B) Numbers 18H01714 and 22H01785 (H.M.), Grant-in-Aid for Scientific Research (C) Number 24K08045 (Y.F.), and for Transformative Research Areas (A) Numbers 20H05881 (Y.O. and S.K.) and 20H05882 (H.M.). This work was also supported by the Tokyo Ohka Foundation for the Promotion of Science and Technology. The discussions with Prof. P. S. Salmon are gratefully appreciated.

Additional information The authors declare no competing financial interests.

References

- 1) G. N. Greaves and S. Sen, *Adv. Phys.* **56**, 1 (2007).
- 2) C. A. Angell, K. L. Ngai, G. B. McKenna, P. F. McMillan and S. W. Martin, *J. Appl. Phys.* **88**, 3113 (2000).
- 3) Y. Onodera, S. Kohara, P. S. Salmon, A. Hirata, N. Nishiyama, S. Kitani, A. Zeidler, M. Shiga, A. Masuno, H. Inoue, S. Tahara, A. Polidori, H. E. Fischer, T. Mori, S. Kojima, H. Kawaji, A. I. Kolesnikov, M. B. Stone, M. G. Tucker, M. T. McDonnell, A. C. Hannon, Y. Hiraoka, I. Obayashi, T. Nakamura, J. Akola, Y. Fujii, K. Ohara, T. Taniguchi and O. Sakata, *NPG Asia Mater.* **12**, 85 (2020).
- 4) S. Kohara, *J. Ceram. Soc. Jpn.* **125**, 799 (2017).
- 5) Y. Onodera, S. Kohara, S. Tahara, A. Masuno, H. Inoue, M. Shiga, A. Hirata, K. Tsuchiya, Y. Hiraoka, I. Obayashi, K. Ohara, A. Mizuno and O. Sakata, *J. Ceram. Soc. Jpn.* **127**, 853 (2019).
- 6) Y. Shi, J. Neufeind, D. Ma, K. Page, L. A. Lamberson, N. J. Smith, A. Tandia and A. P. Song, *J. Non-Cryst. Solids* **516**, 71 (2019).
- 7) S. Kohara, M. Shiga, Y. Onodera, H. Masai, A. Hirata, M. Murakami, T. Morishita, K. Kimura and K. Hayashi, *Sci. Rep.-UK* **11**, 22180 (2021).
- 8) M. Shiga, A. Hirata, Y. Onodera and H. Masai, *Commun. Mater.* **4**, 91 (2023).
- 9) S. Kohara, S. Sato, M. Shiga, Y. Onodera, H. Masai, T. Wakihara, A. Masuno, A. Hirata, N. Kitamura, Y. Idemoto, K. Kimura and K. Hayashi, *J. Ceram. Soc. Jpn.* **132**, 653 (2024).
- 10) A. Hirata, S. Sato, M. Shiga, Y. Onodera, K. Kimoto and S. Kohara, *NPG Asia Mater.* **16**, 25 (2024).
- 11) S. R. Elliott, *Nature* **354**, 445 (1991).
- 12) S. R. Elliott, *J. Phys.-Condens. Mat.* **4**, 7661 (1992).
- 13) A. C. Wright, *J. Non-Cryst. Solids* **179**, 84 (1994).
- 14) P. H. Gaskell and D. J. Wallis, *Phys. Rev. Lett.* **76**, 66 (1996).
- 15) Q. Mei, C. J. Benmore and J. K. R. Weber, *Phys. Rev. Lett.* **98**, 057802 (2007).
- 16) S. Susman, K. J. Volin, D. L. Price, M. Grimsditch, J. P. Rino, R. K. Kalia, P. Vashishta, G. Gwanmesia, Y. Wang and R. C. Liebermann, *Phys. Rev. B* **43**, 1194 (1999).
- 17) S. Kohara, J. Akola, L. Patrikeev, M. Ropo, K. Ohara, M. Itou, A. Fujiwara, J. Yahiro, J. T. Okada, T. Ishikawa, A. Mizuno, A. Masuno, Y. Watanabe and T. Usuki, *Nat. Commun.* **5**, 5892 (2014).
- 18) L. Hennen, V. Cristiglio, J. Kozaily, I. Pozdnyakova, H. E. Fischer, A. Bytchkov, J. W. E. Drewitt, M. Leydier, D. Thiaudière, S. Gruner, S. Brassamin, D. Zanghi, G. J. Cuello, M. Koza, S. Magazù, G. N. Greaves and D. L. Price, *Eur. Phys. J.-Spec. Top.* **196**, 151 (2011).
- 19) L. B. Skinner, C. J. Benmore, J. K. R. Weber, M. C. Wilding, S. K. Tumber and J. B. Parise, *Phys. Chem. Chem. Phys.* **15**, 8566 (2013).
- 20) L. Stixrude and M. S. T. Bukowinski, *Phys. Rev. B* **44**, 2523 (1999).
- 21) P. S. Salmon and A. Zeidler, *Phys. Chem. Chem. Phys.* **15**, 15286 (2013).
- 22) A. Zeidler and P. S. Salmon, *Phys. Rev. B* **93**, 214204 (2016).
- 23) P. S. Salmon, A. Zeidler, M. Shiga, Y. Onodera and S. Kohara, *Phys. Rev. B* **107**, 144203 (2023).
- 24) H. Masai, S. Kohara, T. Wakihara, Y. Shibazaki, Y. Onodera, A. Masuno, S. Sukenaga, K. Ohara, Y. Sakai, J. Haines, C. Levelut, P. Hébert, A. Isambert, D. A. Keen and M. Azuma, *Commun. Chem.* **6**, 269 (2023).
- 25) A. P. Sokolov, A. Kisliuk, M. Soltwisch and D. Quitmann, *Phys. Rev. Lett.* **69**, 1540 (1992).
- 26) L. Börjesson, A. K. Hassan, J. Swenson, L. M. Torell and A. Fontana, *Phys. Rev. Lett.* **70**, 1275 (1993).
- 27) T. Nakayama, *Rep. Prog. Phys.* **65**, 1195 (2002).
- 28) T. Gerber and B. Himmel, *J. Non-Cryst. Solids* **92**, 407 (1987).
- 29) H. Masai, S. Kohara, Y. Onodera, A. Koreeda, K. Saito, E. H. Sekiya and N. Kitamura, *J. Ceram. Soc. Jpn.* **128**, 1038 (2020).
- 30) A. Q. Tool, *J. Am. Ceram. Soc.* **29**, 240 (1946).
- 31) D. B. Fraser, *J. Appl. Phys.* **39**, 5868 (1968).
- 32) R. Brückner, *J. Non-Cryst. Solids* **5**, 123 (1970).
- 33) T. Moynihan, A. J. Easteal, M. A. Debolt and J. Tucker, *J. Am. Ceram. Soc.* **59**, 12 (1976).
- 34) A. Agarwal, K. M. Davis and M. Tomozawa, *J. Non-Cryst. Solids* **185**, 191 (1995).
- 35) M. D. Ediger, C. A. Angell and S. R. Nagel, *J. Phys. Chem.* **100**, 13200 (1996).
- 36) A. Agarwal and M. Tomozawa, *J. Non-Cryst. Solids* **209**, 166 (1997).
- 37) K. Tsujikawa, K. Tajima and M. Ohashi, *J. Lightwave Technol.* **18**, 1528 (2000).
- 38) H. Kakiuchida, K. Saito and A. J. Ikushima, *J. Appl. Phys.* **94**, 777 (2003).
- 39) S. Sen, R. L. Andrus, D. E. Baker and M. T. Murtagh, *Phys. Rev. Lett.* **93**, 125902 (2004).
- 40) V. Lubchenko and P. G. Wolynes, *J. Chem. Phys.* **121**, 2852 (2004).
- 41) A. E. Geissberger and F. L. Galeener, *Phys. Rev. B* **28**, 3266 (1983).
- 42) N. Shimodaira, K. Saito, N. Hiramitsu, S. Matsushita and A. J. Ikushima, *Phys. Rev. B* **71**, 024209 (2005).
- 43) T. Watanabe, K. Saito and A. J. Ikushima, *J. Appl. Phys.* **94**, 4824 (2003).
- 44) R. Shuker and R. W. Gamon, *Phys. Rev. Lett.* **25**, 222 (1970).
- 45) P. F. McMillan, B. T. Poe, P. H. Gillet and B. Reynard, *Geochim. Cosmochim. Ac.* **58**, 3653 (1994).
- 46) V. K. Malinovskiy, V. N. Novikov and A. P. Sokolov, *Phys. Lett. A* **153**, 63 (1991).
- 47) S. R. Elliott, *Europhys. Lett.* **19**, 201 (1992).
- 48) H. Masai, Y. Fujii, N. Kitamura and M. Yamawaki, *J. Non-Cryst. Solids* **576**, 121248 (2022).
- 49) H. Masai, T. Ohkubo, Y. Onodera, Y. Fujii, S. Shimono and A. Koreeda, *J. Ceram. Soc. Jpn.* **133**, 1 (2025).
- 50) H. Kakiuchida, E. H. Sekiya, N. Shimodaira, K. Saito and A. J. Ikushima, *J. Non-Cryst. Solids* **353**, 568 (2007).
- 51) S. Kohara, M. Itou, K. Suzuya, Y. Inamura, Y. Sakurai, Y. Ohishi and M. Takata, *J. Phys.-Condens. Mat.* **19**, 506101 (2007).
- 52) T. E. Faber and J. M. Ziman, *Philos. Mag.* **11**, 153 (1965).
- 53) T. Sonehara, Y. Konno, H. Kaminaga, S. Saikan and S.

- Ohno, *J. Opt. Soc. Am. B* **24**, 1193 (2007).
- 54) T. Sonehara, H. Kaminaga, E. Tatsu, S. Saikan and S. Ohno, *J. Non-Cryst. Solids* **354**, 1768 (2007).
- 55) M. Yamawaki, Y. Kobayashi, K. Hattori and Y. Watanabe, *Jpn. J. Appl. Phys.* **50**, 086301 (2011).
- 56) Y. Onodera, S. Kohara, H. Masai, A. Koreeda, S. Okamura and T. Ohkubo, *Nat. Commun.* **8**, 15449 (2017).
- 57) G. Brauer and G. Boden, *Appl. Phys.* **16**, 119 (1978).
- 58) M. Ono, K. Hara, M. Fujinami and S. Ito, *Appl. Phys. Lett.* **101**, 164103 (2012).
- 59) M. Zanatta, G. Baldi, R. S. Brusa, W. Egger, A. Fontana, E. Gilioli, S. Mariazzi and G. Monaco, *Phys. Rev. Lett.* **112**, 045501 (2014).
- 60) J. Kushibiki, T.-C. Wei, Y. Ohashi and A. Tada, *J. Appl. Phys.* **87**, 3113 (2000).
- 61) H. Masai, *J. Non-Cryst. Solids X* **15**, 100105 (2022).